Applied Catalysis A: General 468 (2013) 410–417

Contents lists available at ScienceDirect

Applied Catalysis A: General

journal homepage: www.elsevier.com/locate/apcata

Selective hydroformylation of olefins over the rhodium supported large porous metal–organic framework MIL-101

Toan Van Vu[a,b,*], Hendrik Kosslick[a,b,*], Axel Schulz[a,b,*], Joerg Harloff[a], Eckhard Paetzold[b], Mathias Schneider[b], Joerg Radnik[b], Norbert Steinfeldt[b], Gerhard Fulda[c], Udo Kragl[a,b]

[a] Institute for Chemistry, University of Rostock, Albert-Einstein-Str. 3a, D-18059 Rostock, Germany
[b] Leibniz Institute for Catalysis (LIKAT), University of Rostock, Albert-Einstein-Str. 29a, D-18059 Rostock, Germany
[c] Center for Electronmicroscopy, Institute of Pathology, University of Rostock, Strempelstr. 14, D-18057 Rostock, Germany

ARTICLE INFO

Article history:
Received 6 May 2013
Received in revised form 21 August 2013
Accepted 9 September 2013
Available online 19 September 2013

Keywords:
Heterogeneous catalysis
Rhodium supported catalyst
Metal–organic framework
MIL-101
Hydroformylation

ABSTRACT

Highly porous and crystalline metal–organic framework MIL-101 has been synthesized and used for the preparation of rhodium supported catalyst. Acetylacetonato(1,5-cyclooctadiene)rhodium(I) has been used as catalyst precursor. The material has been characterized by XRD, XPS, SAXS, FTIR, SEM, TEM, AAS, and nitrogen adsorption. The catalytic properties of Rh@MIL-101 have been investigated in the hydroformylation of olefins with different structure and chain length to the corresponding aldehydes. High conversion and selectivity to *n*-aldehydes have been achieved in the hydroformylation of *n*-alk-1-enes. The obtained results show that the rhodium species are highly dispersed and preferentially located at internal and less accessible sites at the supertetrahedral units.

1. Introduction

Metal–organic frameworks (MOFs) are well-known crystalline inorganic–organic hybrid materials. They possess diverse desirable properties such as high specific surface areas, tunable pore sizes, and the possibility to functionalize, modify, or exchange organic linkers as well as metal components, which make MOFs special compared to common micro and mesoporous materials [1–6]. The discovery of these materials with outstanding features has opened a variety of new opportunities for potential applications in gas storage, separation, and heterogeneous catalysis [7–17].

The extra-large porous metal–organic framework, MIL-101, has been discovered and described by Férey et al. [2]. MIL-101 exhibits an extremely high surface area of up to 5900 m^2/g and thermal stability in air up to 275 °C. The structure of the MIL-101 is composed of inorganic trimeric octahedral chromium metal building blocks and alternative arranged organic 1,4-benzene dicarboxylate (BDC) linker as primary units. They form so-called supertetrahedral secondary building units (ST) building up the ordered and highly porous crystalline framework of the chemical composition $[(Cr_3X(H_2O)_2O(O_2C–C_6H_4–CO_2)]_3{\cdot}25H_2O$, with X = F, OH. The pore system of MIL-101 consists of two different sized large cages of ca. 29 Å and 34 Å internal diameter and pore volumes of ca. 12.700 $Å^3$ and 20.600 $Å^3$, respectively. The smaller one is accessible via pentagonal windows of ca. 12 Å size. The larger cage has both pentagonal (12 Å) and hexagonal windows of ca. 14.5 × 16 Å size. The two large cages are delimited by 20 and 28 ST units, respectively. The ST units are microporous with trigonal pore openings of ca. 8.6 Å and can be considered as "side pockets" of the walls of the large cavities.

Due to high porosity, extra-large pore sizes and comparatively high thermal and chemical stability, the metal–organic framework MIL-101 has attracted attention as potential catalytic material. The strict alternative arrangement of inorganic and organic constituents facilitates the formation of highly dispersed noble metal species and the formation of catalytic interesting single sites.

MIL-101 based catalysts have been found to be active in a couple of different reactions. Making use of acid-base properties and the presence of coordinative unsaturated sites, the catalytic properties of MIL-101 have been tested in the base and acid catalyzed Knoevenagel condensation of benzaldehyde with ethyl cyanoacetates over amino-functionalized MIL-101 [18] and polyoxometallate (POM) loaded MIL-101 as well as esterification of *n*-butanol with acetic acid [19]. The esterification of *n*-butanol with acetic acid has been

* Corresponding authors. Tel.: +49 381 498 6384; fax: +49 381 498 6382.
E-mail addresses: vantoan.vu@uni-rostock.de, vutoan_hn@yahoo.com (T. Van Vu), hendrik.kosslick@uni-rostock.de (H. Kosslick), axel.schulz@uni-rostock.de (A. Schulz).

0926-860X/$ – see front matter © 2013 Elsevier B.V. All rights reserved.
http://dx.doi.org/10.1016/j.apcata.2013.09.011

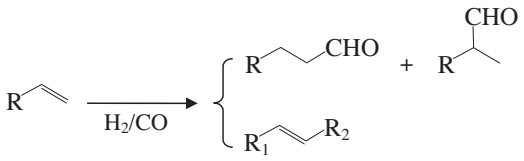

Fig. 1. Scheme of the hydroformylation of *n*-alk-1-ene with synthesis gas to *n*- and *i*-aldehydes and formation of double bond shifted internal alkene side product.

carried out also over Brønsted acidified catalyst [13]. The Lewis acidity of MIL-101 has been used in the cyanosilylation of benzaldehyde with trimethylsilylcyanide [8].

MIL-101 catalysts have been shown to be active also in oxidation reactions like the selective oxidation of sulfides with hydrogen peroxide to the corresponding sulfoxides, which has been assigned to the activity of coordinative unsaturated metal sites (CUS) [20]. Furthermore, the catalytic activity has been investigated in the direct oxidation of alkenes to carboxylic acids with H_2O_2 [21], the selective oxidation of tetralin to tetralone using *tert*-butyl hydroperoxide using a MIL-101 coated monolith catalyst [22], the epoxidation of alkenes with H_2O_2 over POM supported MIL-101 [23,24] and other selective oxidations [25]. The performance of MIL-101 (Cr, Fe) in liquid-phase processes as the selective oxidation of hydrocarbons with green oxidants like O_2 and *tert*-butyl hydroperoxide as well as the coupling reaction of organic oxides with CO_2 has been reviewed recently [26].

The catalytic performance in the hydrogenation has been tested using palladium supported MIL-101 catalysts. MIL-101 has been found to be a remarkably stable support for palladium in hydrogenation of styrene and cyclooctene showing significantly higher activity than e.g. of palladium supported activated carbon catalyst [8]. Pd@MIL-101 has been also used as multifunctional catalyst in the one-step synthesis of methyl isobutyl ketone by multi-step hydrogenation reaction starting with acetone [27], the cyclization of citronellal to isopulegol, and the one-pot tandem isomerization/hydrogenation of citronellal to menthol [28].Recently, Pd@MIL-101 and Pt@MIL-101 as multifunctional catalysts have been also tested in the synthesis of secondary arylamines, quinolines, pyrrols, and 3-arylpyrrolidines [29]. High palladium loaded MIL-101 catalysts containing different sized palladium nanoparticle have been applied for the selective hydrogenation of ketones to the corresponding alcohols [30]. Highly dispersed single site platinum loaded NH_2–MIL–101(Al) catalysts have been prepared by deposition of the metal on the phosphotungstic acid pre-loaded metal–organic framework. The catalyst showed high activity in the CO oxidation and improved selectivity compared to platinum supported alumina [31].

The properties of MIL-101 make this material also interesting for use in the hydroformylation of olefins to aldehydes. In the industrial scale, the hydroformylation is one of the most important homogeneous catalyzed reactions [32,33], in which synthesis gas is added to an alkene to produce linear and branched aldehydes as shown in Fig. 1 [34]. Linear aldehyde, a more valuable product, can be used for the production of alcohols. Approximately 9 million metric tons of aldehydes and alcohols are annually produced using the hydroformylation reaction. They are starting materials for the synthesis of plasticizers, detergents, adhesives, solvents, pharmaceuticals as well as agrochemicals [5,35,36].

Both cobalt and rhodium complexes are used in the industrial homogeneous catalyzed hydroformylation. The enhancement of reaction rate and selectivity by ligand design as well as process optimization has received great attention [37]. Even though the traditional hydroformylation is effective, there is an interest in the heterogenization of organic synthesis processes. Therefore, research efforts are aimed at the immobilization of metal complexes [32,38]. Until now, several support materials have been tested. They include materials such as silica, alumina, zeolite, activated carbon, supported aqueous phase catalyst (SAPC), and polymeric organic as well [32,39–45]. However, there are some limits of supports in this heterogeneous hydroformylation due to the loss of activity, low thermal stability or complicated procedure to synthesize the catalyst [38].

In this study, the rhodium supported MIL-101catalyst, Rh@MIL-101, is investigated in the hydroformylation of different olefins. In detail, *n*-alk-1-enes of different chain lengths are used. Furthermore, some bulky and less flexible olefins are included in order to evaluate the influence of structure of the porous metal–organic framework. The purpose is to check the catalytic performance of the Rh@MIL-101 catalyst using hydroformylation as a test reaction.

2. Materials and methods

2.1. Material preparation

2.1.1. MIL-101 synthesis

MIL-101 was hydrothermally synthesized in the presence of TMAOH (tetramethylammonium hydroxide) based on literature [46] using an improved work up procedure.

As starting materials $Cr(NO_3)_3{\cdot}9H_2O$ (chromium(III) nitrate), H_2BDC (terephthalic acid), and 0.05 M TMAOH were used. Typically, 0.62 g of H_2BDC (Merck, ≥98%) was added to 18.75 mL of aqueous 0.05 M TMAOH (Sigma-Aldrich, ≥97%) and vigorously stirred for 30 min at room temperature. Then 1.5 g of $Cr(NO_3)_3{\cdot}9H_2O$ was added to this mixture and stirred for further 1 h. Next, this reaction mixture was transferred into a 120 mL Teflon-lined autoclave. It was heated at the rate of 2 °C/min up to 180 °C and maintained at this temperature for 24 h under static condition.

After reaction, the autoclave was allowed to cool down to room temperature. The green reaction product was recovered by centrifugation at 4000 rpm for 25 min. Thereafter, the precipitate was suspended in water. The white large elongated unreacted H_2BDC crystals were separated from the reaction product by centrifugation at 1600 rpm for 5 min. The remaining opaque green mixture was further centrifuged at 4000 rpm for 25 min to recover the MIL-101. The obtained product was worked up four times using the same procedure. Finally, the obtained green MIL-101 sample was dried at 90 °C.

2.1.2. Rhodium loading

An amount of 1.85 g MIL-101 was added to a solution containing 15.7 mL of acetonitrile (Baker), 11.2 mL of toluene (Merck), and 5.61 mg of [(acetylacetonato)(1,5-cyclooctadiene)] rhodium(I) with a rhodium content of ca. 33%. The mixture was stirred and slowly heated to ca. 70 °C in order to evaporate the solvents gradually. The material became dry after ca. 2.5 h. Next, the green powder was washed three times with 5 mL of toluene. After washing, the obtained Rh@MIL-101 supported catalyst was dried at 90 °C.

2.2. Material characterization

MIL-101 and its rhodium loaded form, Rh@MIL-101, were characterized by XRD, XPS, SAXS, IR, SEM, TEM, AAS, and nitrogen sorption measurements. The XRD investigation was carried out on a STADI-P X-ray diffractometer (STOE) using monochromatic Cu*K*α radiation (λ = 1.5418 Å). The rhodium content of the Rh@MIL-101 supported catalyst was determined by atomic absorption spectrometry with an AAS-Analyst 300 device (Perkin Elmer). A nitrous oxide/acetylene or air/acetylene mixture was used for the burner system. XPS measurements were done at an ESCALAB220iXL spectrometer (Thermo Fisher) with monochromatic Al K_α radiation (E = 1486.6 eV). The samples were fixed on a stainless steel

sample holder with double adhesive carbon tape. The binding energies were referred to C_{1s} at 284.8 eV. For determination of the binding energy and peak area the peak were fitted with Gaussian–Lorentzian curves. The base pressure of the UHV chamber was below 1×10^{-7} Pa. SAXS measurements were carried out with a Kratky-type instrument (SAXSess, Anton Paar, Austria) operated at 40 kV and 50 mA in slit collimation using a two-dimensional CCD detector ($T = -40\,^{\circ}C$). The 2D scattering pattern was converted into a one-dimensional scattering curve as a function of the magnitude of the scattering vector $q = (4\pi/\lambda)\sin(\theta/2)$ with SAXSQuant Software (Anton Paar). A Göbel mirror was used to convert the divergent polychromatic X-ray beam into a collimated line-shaped beam of Cu K_α radiation ($\lambda = 0.154$ nm). Slit collimation of the primary beam was applied in order to increase the flux and to improve the signal quality. IR spectroscopic measurements were recorded on a Nicollet 380 FTIR spectrometer in attenuated total reflection mode using a smart orbit ATR device. The resolution was ca. 4 cm^{-1}. The powders were measured as obtained. SEM images were received by a DSM 960A electron microscope operating at 10 kV (Carl Zeiss, Oberkochen) with a resolution of 4 nm. The sample was suspended in water and put into an ultrasonic bath in order to disperse the solid in water as much as possible. Then a small and representative drop of the sample mixture was deposited on a sample plate. After drying, the plate containing very small particles of sample was coated with a very thin layer of gold by using plasma distribution method. Next, the sample plate was put into the sample box for SEM investigation. Before scanning, the sample inside the box was under high vacuum (ca. 2×10^{-5} hPa). SEM image with the high magnification of 30,000 was taken with speed of 200 μm/pixel in accordance with the scanning time of ca. 3 min. TEM measurements were performed with a LIBRA 120 transmission electron spectrometer (Carl Zeiss, Oberkochen) at 120 kV with a resolution of 0.3 nm. Prior to TEM investigations, similar to SEM, the sample was well dispersed in water and then deposited on copper grids. Images were recorded with a digital camera with 2000 × 2000 pixels. Nitrogen adsorption and desorption measurement was performed on an ASAP 2010 sorption system. Before measurement, the solvent in the sample was removed by heating and pumping under reduced pressure at ca. 150 °C. Nitrogen adsorption measurements were carried out at 77 K (−196 °C).

2.3. Catalytic testing

The linear alk-1-enes as *n*-hex-1-ene (Sigma-Aldrich, ≥97%), *n*-oct-1-ene (Sigma-Aldrich, ≥98%), *n*-dec-1-ene (Acros, ≥95%), *n*-dodec-1-ene (Acros, 93–95%), and *n*-hexadec-1-ene (Acros, ≥98%) were used in the hydroformylation of *n*-alkenes over Rh@MIL-101 supported catalyst. Additionally, some bulky olefins like 2,4,4-trimethylpentene (Sigma-Aldrich, ≥99%), cyclohexene (Sigma-Aldrich, ≥99%), and cyclooctene (Acros, ≥95%) or the less flexible hexa-1,5-diene (Janssen, ≥98%) were used. The catalytic activity of the parent MIL-101 alone (without rhodium) has been checked in blank experiments.The catalytic tests were carried out in the following way. The mixture containing the substrate (olefin), the solvent (toluene), and the catalyst was filled into a 100 mL PARR reactor equipped with a gas introduction stirrer. Next, the reactor was shortly evacuated to remove the air and moisture. Then the autoclave was refilled with argon. After purging with argon, the reactor was loaded with synthesis gas ($CO/H_2 = 1$) at a pressure of 50 bar at room temperature. The autoclave was heated under stirring at 1000 rpm and maintained at a temperature of 100 °C during the course of reaction.

Typically, in hydroformylation of *n*-hex-1-ene, the reactor was loaded with 12.5 mL of the olefin, 30 mL of toluene, and ca. 90 mg of the Rh@MIL-101 catalyst. The molar olefin/catalyst ratio was ca. 70,000/1 based on rhodium. The other experiments with different olefins were carried out in a similar way. The molar olefin/catalyst ratio was kept constant.

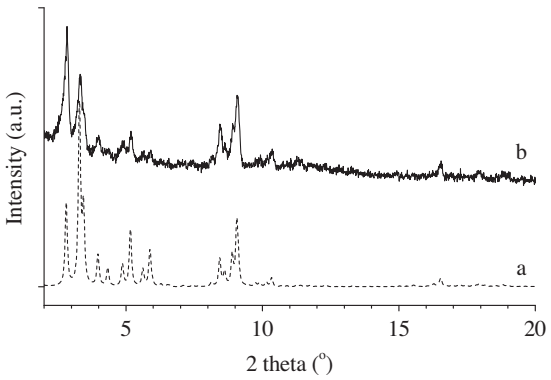

Fig. 2. XRD pattern of MIL-101 (a) calculated pattern and (b) experimental pattern.

3. Results and discussion

3.1. Materials

The crystallinity and structure of the synthesized MIL-101 sample was checked by powder X-ray diffraction (Fig. 2). The obtained diffraction pattern is in agreement with the simulated one confirming the formation of the MIL-101 structure [2,46]. The diffractogram shows resolved and narrow reflections indicating a well-crystallized material.

The Cr_{2p} XP spectra of the starting MIL-101 and Rh@MIL-101 are shown in Fig. 3. They show doublet signals with peak maxima arising at 585.32 eV and 576.02 eV in case of MIL-101 and 583.98 eV and 574.68 eV in case of Rh@MIL-101, respectively. This amounts to a significant shift of the signal maxima of 1.34 eV to lower energy. The shift indicates strong interaction of the rhodium with chromium metal sites in the MOF structure even the rhodium loading was low. A less pronounced shift of 1.13 eV is observed with the O_{1s} signal. Whereas, only minor changes of 0.07–0.49 eV to lower energy are found with the C_{1s} signal, as shown in Table 1. The shifts confirm the location of the rhodium species in the framework nearby the

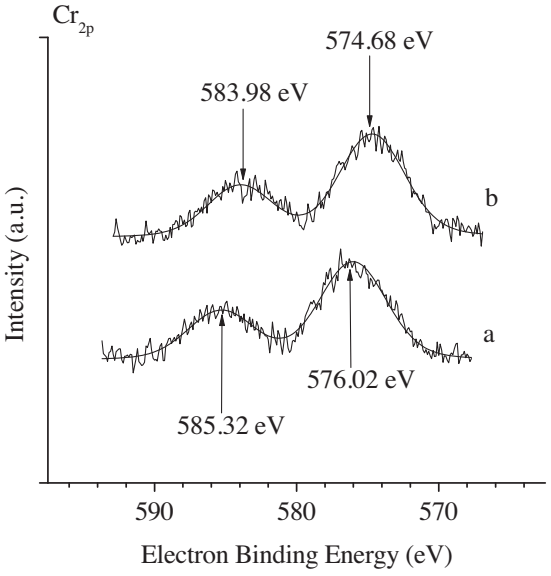

Fig. 3. XPS spectra showing the Cr_{2p} doublet signal of (a) MIL-101 support and (b) Rh@MIL-101 catalyst.

Table 1
Electron binding energy of elements of MIL-101 before and after loading rhodium species.

Peak	Binding energy (eV)	
	MIL-101	Rh@MIL-101
C_{1s}	281.29	280.80
	284.82	284.77
	289.12	289.05
O_{1s}	530.80	529.67
Cr_{2p}	576.02	574.68
	585.32	583.98

chromium and also oxygen. The rhodium loading was too low to be detected by XPS.

FTIR spectra of MIL-101 sample and Rh@MIL-101 supported catalyst are shown in Fig. 4. They are dominated by the vibration bands of the linker. They are well resolved and show the typical vibration bands usually observed of benzene carboxylate. The vibration bands occurring between 1630 cm^{-1} and 1390 cm^{-1} are related to vibrations of the carboxylate anion groups (1630–1500 cm^{-1}), C–O–H bending, or stretch in-plane bending modes (1440–1395 cm^{-1}) and deformation modes (1420–1340 cm^{-1}). CO–O and C–O stretching vibrations appear between ca. 1250 cm^{-1} and 1040 cm^{-1}. The bands below 900 cm^{-1} belong to different bending vibration bands of the C–H bonds (900–800 cm^{-1}) and =C–H deformation bands of the benzene ring (770–670 cm^{-1}). The vibration bands of the carboxy groups might be overlapped by less intensive C=C stretch and ring vibrations of the benzene. Vibration bands of free carboxy acid appearing at 1760–1690 cm^{-1} are not observed. The latter finding confirms the purity and stability of the prepared MIL-101. Interestingly, the rhodium loading causes only minor shifts (ca. 1 cm^{-1}) of the vibration bands to lower frequency. The largest shift of up to 3 cm^{-1} are observed with the carboxy vibration band at ca. 1628 cm^{-1}. Additionally, a splitting of the vibration band located at 745 cm^{-1} is observed. This finding is in line with a location of the rhodium nearby the chromium sites as indicated by XPS. In contrast, significant shifts of the BDC linker vibrations to lower frequency of up to 15 cm^{-1} have been observed with MOF-5 with similar low rhodium loading [5].

The SEM image of MIL-101 shows the formation of the well-shaped MOF particles during the course of the hydrothermal synthesis (Fig. 5). The particles are agglomerated and in size of ca. 150–250 nm. The TEM measurement gives no indication of the formation of larger rhodium particles indicating that these active rhodium species are well dispersed in the MOF framework.

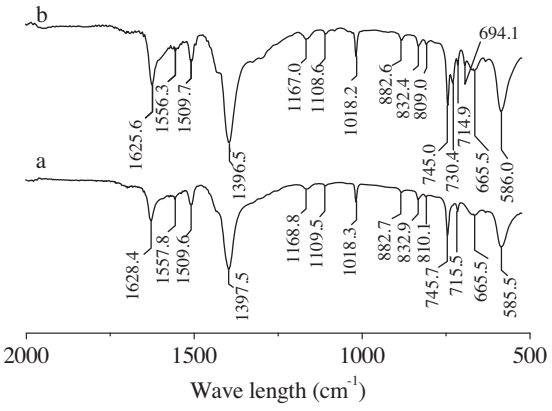

Fig. 4. Mid FTIR spectra of (a) MIL-101 and (b) Rh@MIL-101 catalyst in the spectral range of organic linker vibrations.

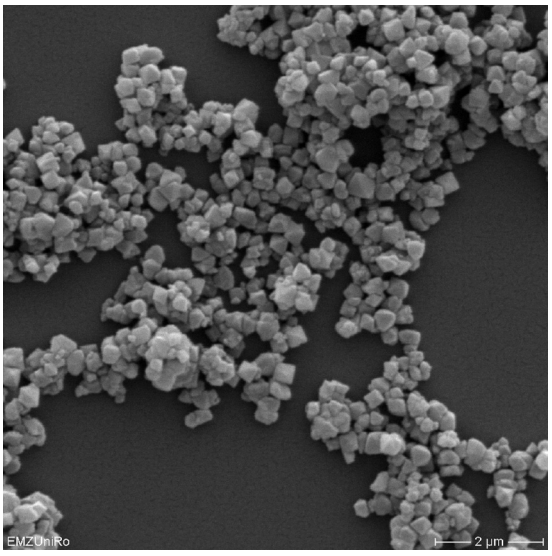

Fig. 5. SEM image of Rh@MIL-101 catalyst crystals.

With an actual Rh loading of 0.15 wt% determined by AAS, ca. 1.2% of the trimeric chromium sites are occupied by Rh assuming an atomic (single site) metal distribution in the framework. This loading is high enough to provide a sufficient amount of single site rhodium species. The two large cages are surrounded by 20 or 28 ST units, which are constructed by four trimeric chromium sites. High dispersion of loaded rhodium is also indicated by chromium XPS data discussed above, which show a substantial shift of the chromium signals even after low Rh loading.

SAXS measurements of the parent MIL-101 and Rh@MIL-101 (0.15 wt% Rh) catalyst have been performed to get additional information about the rhodium species. Because the SAXS data of MIL-101 and Rh@MIL-101 catalyst did not differ, higher loadings of 1% and 2% of Rh on MIL-101 have been included. The scattering curves of MIL-101 and Rh@MIL-101 (1 wt% Rh) in the q-range between 0.1 and 1, which is plotted as a log–log plot of intensity I vs. scattering vector q, are shown in Fig. 6. They are nearly straight lines. The slope of log I vs. log q plot in the Porod regime [47,48] is between 3.8 and 4. The observed scattering is attributed to the particle surface structure of the MIL-101 particles whereas a slope near 4 indicates a smooth particle surface. The presence of nanoparticles would add an additional intensity in the q-range

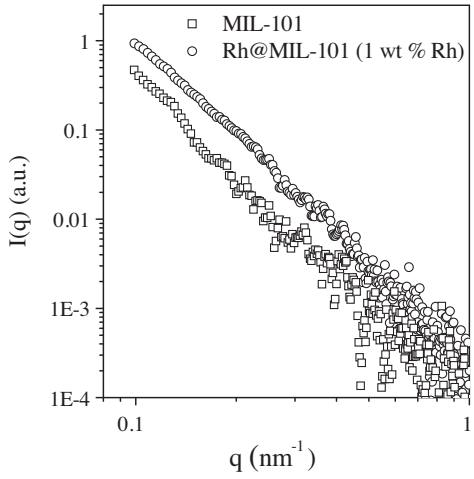

Fig. 6. Scattering curves obtained from SAXS measurements of MIL-101 and Rh@MIL-101.

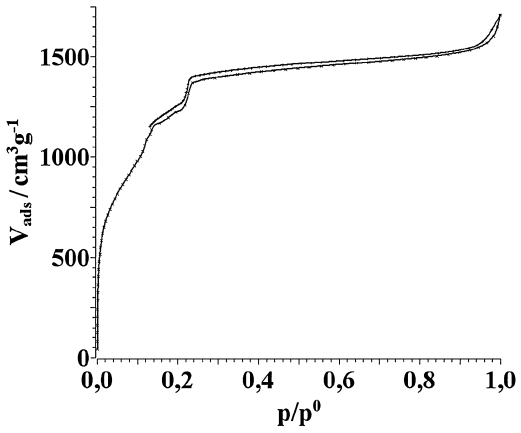

Fig. 7. Nitrogen adsorption and desorption isotherm of the metal–organic framework MIL-101 support measured at −196 °C.

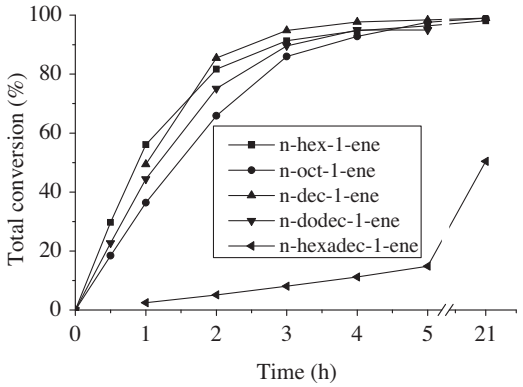

Fig. 8. Total conversion of *n*-alk-1-ene in the hydroformylation to aldehydes and double bond shifted internal alkene side products over Rh@MIL-101 catalyst. Reaction conditions: olefin/Rh = 70,000/1, T = 100 °C, and P = 50 bar.

giving rise to a curved-shape of the plot [49]. In none of the samples additional scattering of small nano-sized Rh structures could be detected which are inline with above discussed findings of high dispersion of rhodium in the MOF.

The nitrogen adsorption–desorption isotherm of the sample is shown in Fig. 7. The adsorption isotherm shows three distinct adsorption steps. At a very low relative pressure up to $p/p_0 = 0.01$, the uptake curve shows a very steep increase. It is assigned to the filling of micropores. Between the relative pressure of $p/p_0 = 0.01$–0.2, the slope of the adsorption isotherm decreases. This second step is related to the filling of small mesopores followed by a third step near $p/p_0 = 0.25$ of final pore filling. Further nitrogen uptake at the high relative pressure above $p/p_0 = 0.8$ is due to textural porosity. The overall course of the adsorption isotherm is characteristic for MIL-101 structure [50]. The well resolved adsorption steps of the isotherm and the high uptake confirms the formation of the well crystallized MIL-101. The BET surface area of the prepared MIL-101 is 4703 m^2/g, which is a high value compared to the other porous support materials. The specific pore volume amounts to 2.38 cm^3/g. The textural data also confirm the successful removal of excessive and difficult to remove terephthalic acid from the reaction mixture by the used repeated centrifugation method.

3.2. Catalysis

The catalytic performance of the Rh@MIL-101 supported catalyst has been investigated using the hydroformylation of linear alkenes with different chain lengths. The analysis of the reaction products shows that beside *n*- and *i*-aldehydes as the desired reaction products also double bond shifted internal alkenes are formed as side products by isomerization. A notable hydrogenation of alkenes to saturated alkanes was not observed. The blank experiments with *n*-hex-1-ene and *n*-oct-1-ene show that the parent MIL-101 (without rhodium) does not catalyze the double bond isomerization of *n*-alk-1-enes to internal alkenes or the hydroformylation of alkenes to aldehydes even after 21 h of reaction.

The dependence of the total conversion on the reaction time of the different *n*-alk-1-ene as *n*-hex-1-ene, *n*-oct-1-ene, *n*-dec-1-ene, *n*-dodec-1-ene, and *n*-hexadec-1-ene over Rh@MIL-101 are shown in Fig. 8. With the exception of *n*-hexadec-1-ene, the reactions proceed fast. Total conversions of ca. 35–55% are already achieved after 1 h of reaction depending on the starting *n*-alk-1-ene. Ca. 90% of conversion is achieved after 3 h of reaction for all used alkenes. The high activity of the catalyst despite of the low Rh loading points to the presence of highly dispersed single site species. The formation of uniform and small Rh species is facilitated by a defined support with structural uniformity of metal oxide surfaces combined with well separated inorganic and organic components as present in MOF and the use of Rh(acac) precursor. Thereby, the acetylacetonato (acac) ligand of the metal complex is replaced by oxygen of the metal sites [51,52]. The reaction of the present OH groups located at chromium site assists the replacement of the acac ligand from the Rh precursor and formation of metal–O bonds as shown with supported zeolites [52].

With exception of *n*-oct-1-ene, the conversions systematically decrease with growing chain lengths of the *n*-alk-1-ene in the order: *n*-hex-1-ene > *n*-dec-1-ene > *n*-dodec-1-ene > *n*-oct-1-ene ≫ *n*-hexadec-1-ene, after 1 h of reaction. The conversion of *n*-oct-1-ene is lower than that of the larger molecules *n*-dec-1-ene and *n*-dodec-1-ene. Very low conversion is observed with the bulky *n*-hexadec-1-ene compared to *n*-dodec-1-ene. The conversion of *n*-hexadec-1-ene slowly increases with prolonged time of reaction. The slow conversion points to a mass transfer hindrance of this large molecule due to the limited window sizes of 12 Å and 14.5 Å of the pores in the MIL-101 structure and/or limited access to the active sites.

In Fig. 9 is shown the selectivity to aldehydes in dependence of the reaction time observed with *n*-alk-1-enes. The selectivity is only ca. 20% in case of *n*-hex-1-ene, whereas it is nearly 30% in case of the longer chain molecules as *n*-oct-1-ene, *n*-dec-1-ene, and *n*-dodec-1-ene. That means, ca. 80% or 70% of reaction products belong to double bond isomerized internal alkenes. Rh itself could favor this isomerization. Interestingly, the aldehyde selectivity is nearly unchanged during the course of reaction, even after 21 h (Fig. 9). This finding reveals that double bond shifted internal alkenes, accounting for 70–80% of the reaction mixtures, are

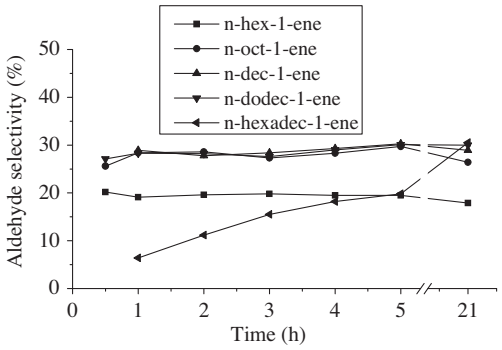

Fig. 9. Selectivity to aldehydes in the hydroformylation of *n*-alk-1-ene over Rh@MIL-101 catalyst. Reaction conditions: olefin/Rh = 70,000/1, T = 100 °C, and P = 50 bar.

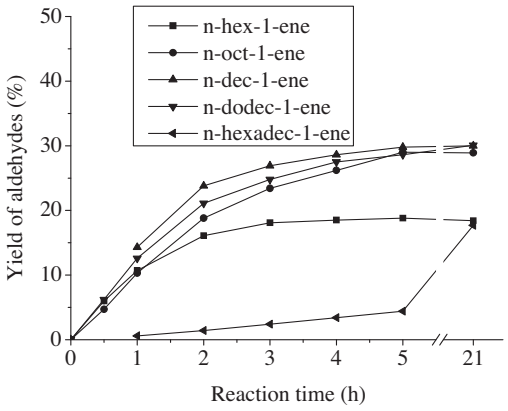

Fig. 10. Yield of aldehyde in the hydroformylation of *n*-alk-1-ene over Rh@MIL-101 catalyst. Reaction conditions: olefin/Rh = 70,000/1, T = 100 °C, and P = 50 bar.

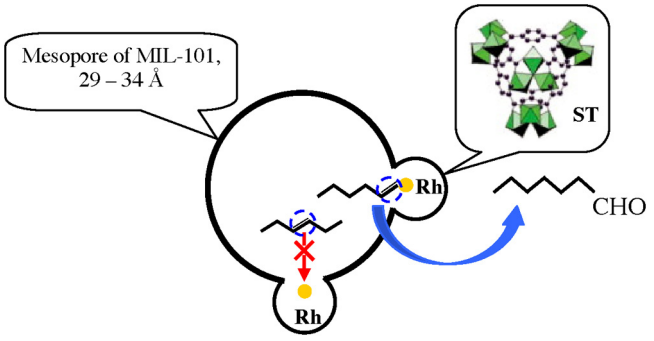

Fig. 11. Schematic representation of large cages and supertetrahedral (ST) side pockets of MIL-101. Proposed location of dispersed Rh active sites on less accessible position at the microporous ST forming the walls of the large cages of MIL-101 leading to limited access of converted internal alkene compared to the starting terminal.

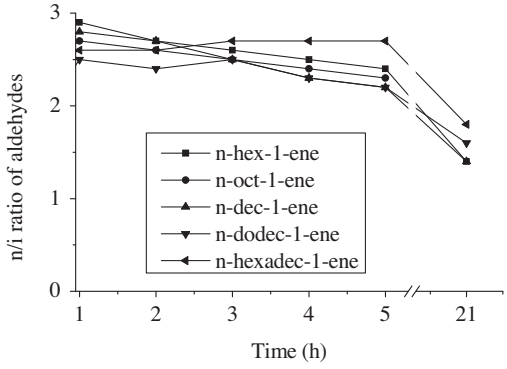

Fig. 12. *n*/*i*-Aldehyde ratio in the hydroformylation of *n*-alk-1-ene over Rh@MIL-101 catalyst. Reaction conditions: olefin/Rh = 70,000/1, T = 100 °C, and P = 50 bar. *n*-alk-1-ene.

nearly not converted to the corresponding aldehydes over Rh@MIL-101. This result is different from the hydroformylation performance observed with the Rh@MOF-5 [5]. In the latter, a large amount of *i*-aldehydes is formed from double bond shifted internal alkenes present in the reaction mixture.

The selectivity behavior is reflected in the yield of aldehydes (Fig. 10). During the first 3 h to 4 h of reaction the yields increase in parallel with the conversion. However, the yields are not further increased after achieving nearly complete conversion (>90%) of the *n*-alk-1-enes. Even after prolonging the reaction time to 21 h the yields are only slightly changed with exception of the *n*-hexadec-1-ene. As mentioned above, the mass transfer of this large *n*-hexadec-1-ene molecule is decreased and the access to the active sites is hindered due to the shielding of the C=C double bond by the surrounding of large alkyl chain. Therefore, the initial aldehyde selectivity is comparatively low and slowly increased with reaction time. The finding, that the internal alkenes are hardly converted to the corresponding *i*-aldehydes, points to a hindered access of these molecules to the active rhodium sites of the MOF. This is apparently surprising because the MIL-101 framework is highly porous and contains extra-large cages. But the result can be explained by a preferred location of the active rhodium at the ST units. These units are microporous [50] limiting approach and access of the olefins to the Rh active sites. As known from related crystalline microporous zeolite structures, small windows and cages are preferred sites for metal ions [53]. They are energetically favored due to short interaction distances and the enhanced number of surrounding neighbored atoms. Therefore, it is plausible to assume that the catalytic active and highly dispersed rhodium species are located at these sites in the supertetrahedra. These window sites are less accessible which explains the limited conversion of internal alkenes R_1–CH=CH–R_2 to aldehydes where the double is located inside of the molecule and shielded by space demanding alkyl groups on both of the sides. Therefore, the approach of C=C group to the active site is hindered. In contrast, in *n*-alk-1-ene, the double bond is located at the head of the molecule R–CH=CH_2 and can be exposed to the active sites (Fig. 11).

Interestingly, the *n*-oct-1-ene has been found to be less active than the larger *n*-dec-1-ene and *n*-dodec-1-ene (Fig. 8). This finding is also observed in the hydroformylation of *n*-alk-1-enes over Rh@MOF-5 and Rh@IRMOF-3 [54]. With MOF-5 and IRMOF-3 supports, less large porous (microporous) metal–organic frameworks compared to MIL-101, the activity differences are more pronounced. A possible reason could be that the relative long and straight *n*-oct-1-ene (ca. 10 Å in length) is difficult to arrange at the active sites in the limited space of the pores.

The *n*/*i* ratios of aldehydes are presented in Fig. 12. They are ca. 2.5–3 during 1–3 h of reaction. The MIL-101 framework shows improved *n*-aldehyde selectivity. The *n*/*i*-aldehyde ratios decrease to 1.5–1.8 after prolonged reaction time, although the yields of aldehydes are only slightly changed. The decrease of the *n*/*i*-aldehyde ratio is due to the aldol condensation side reaction after long time of reaction yielding the corresponding unsaturated aldehydes preferentially from *n*-aldehyde. GS/MS analysis of reaction solutions after 5 h and 21 h of *n*-hex-1-ene hydroformylation shows favored aldol condensation of *n*-heptanal (Table 2). The loss of aldehydes by aldol condensation is in part compensated by the formation of aldehydes from remaining *n*- and internal alkenes in reaction solution (Table 2). Therefore, the yield of aldehyde is slightly decreased after prolonged reaction time (Fig. 10). The aldol condensation side reaction is accelerated by the acid sites of the MIL-101, which is of ca. 1 mmol/g created at coordinative unsaturated chromium

Table 2
Detail of product mixture in hydroformylation of *n*-hex-1-ene after 5 h and 21 h of reaction.

Substrate/product in reaction product	Reaction time	
	5 h	21 h
n-Hex-1-ene (%)	3.6	1.8
Internal hexenes (%)	75.9	74.5
n-Aldehyde (%)	13.5	10.1
i-Aldehydes (%)	5.9	6.8
Aldol condensation products (%)	0.6	4.6*
Sum of aldehydes (%)	19.4	16.9

* Aldol condensation products containing 83% of H_3C–$(CH_2)_5$–CH=C(CHO)–$(CH_2)_4$–CH_3.

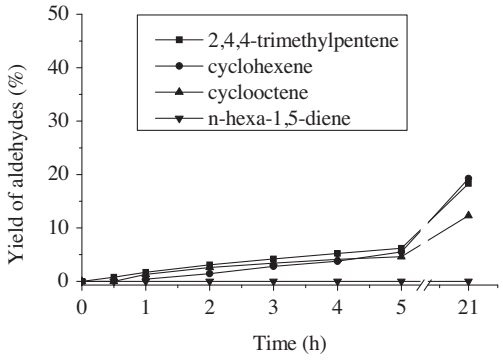

Fig. 13. Yield of aldehyde in the hydroformylation of bulky/less flexible olefin over Rh@MIL-101 catalyst. Reaction conditions: olefin/Rh = 70,000/1, T = 100 °C, and P = 50 bar.

metal sites in MOF structure [50]. As a result, the *n*/*i*-aldehyde ratio decreases after long time of reaction.

The steric constrains giving rise to limited access to rhodium sites in the MIL-101 framework have been further studied using different bulky alkenes as 2,4,4-trimethylpentene (TMP), cyclohexene, cyclooctene, and the less flexible hexa-1,5-diene. The yields of aldehydes in these hydroformylation reactions are shown in Fig. 13. The TMP, cyclohexene, and cyclooctene are slowly converted to aldehydes. However, hexa-1,5-diene is not converted although one C=C double bond is located in "head" position like in *n*-hex-1-ene and the molecules are of similar size. The hexadiene, as a typical diene, is a very stiff bar-shaped molecule and the diene can act as a poison [55].

4. Conclusion

Well crystallized and highly porous metal–organic framework MIL-101 has been synthesized and used for the preparation of Rh@MIL-101 catalyst. The catalytic performance has been studied in the hydroformylation of different sized and shaped olefins to the corresponding aldehydes. Despite low Rh loading, the catalyst is highly active which is assigned to the high dispersion and formation single site Rh species in the inorganic organic hybrid framework. The catalyst behaves selective. The *n*/*i*-aldehyde ratios achieve values of up to 3. The bulky olefins are slowly converted, even though MIL-101 is a highly porous support containing mesopores and extra-large cages. Especially, the double bond shifted internal alkenes are hardly converted to the corresponding aldehydes. The observed selectivity is ascribed to the location of catalytic active rhodium species at internal framework sites of the microporous supertetrahedra, which renders approach of molecules to the active sites more difficult.

Acknowledgment

The authors gratefully acknowledge the excellent assistance of Mrs. Susann Buchholz, Mrs. Susanne Schareina, and Dr. Christine Fischer for analysis of reaction products. This work was in part supported by the German Academic Exchange Service (DAAD), the International Bureau of the Federal Ministry of Education and Research (BMBF, Germany), and granted from the Ministry of Education and Training of Vietnam (MOET, Vietnam) which is gratefully acknowledged by the authors.

References

[1] M. Eddaoudi, J. Kim, N. Rosi, D. Vodak, J. Wachter, M. O'Keeffe, O.M. Yaghi, Science 295 (2002) 469–472.
[2] G. Férey, C. Mellot-Draznieks, C. Serre, F. Millange, J. Dutour, S. Surblé, I. Margiolaki, Science 309 (2005) 2040–2042.
[3] M. Sabo, A. Henschel, H. Frode, E. Klemm, S. Kaskel, J. Mater. Chem. 17 (2007) 3827–3832.
[4] A. Huang, W. Dou, J. Caro, J. Am. Chem. Soc. 132 (2010) 15562–15564.
[5] T.V. Vu, H. Kosslick, A. Schulz, J. Harloff, E. Paetzold, H. Lund, U. Kragl, M. Schneider, G. Fulda, Microporous Mesoporous Mater. 154 (2012) 100–106.
[6] M. Dogru, A. Sonnauer, A. Gavryushin, P. Knochel, T. Bein, Chem. Commun. 47 (2011) 1707–1709.
[7] S. Hermes, M.-K. Schröter, R. Schmid, L. Khodeir, M. Muhler, A. Tissler, R.W. Fischer, R.A. Fischer, Angew. Chem. Int. Ed. 44 (2005) 6237–6241.
[8] A. Henschel, K. Gedrich, R. Kraehnert, S. Kaskel, Chem. Commun. (2008) 4192–4194.
[9] J. Juan-Juan, J.P. Marco-Lozar, F. Suárez-García, D. Cazorla-Amorós, A. Linares-Solano, Carbon 48 (2010) 2906–2909.
[10] O. Shekhah, J. Liu, R.A. Fischer, C. Woll, Chem. Soc. Rev. 40 (2011) 1081–1106.
[11] D. Saha, S. Deng, Int. J. Hydrogen Energy 34 (2009) 2670–2678.
[12] J. Gascon, U. Aktay, M.D. Hernandez-Alonso, G.P.M. van Klink, F. Kapteijn, J. Catal. 261 (2009) 75–87.
[13] M.G. Goesten, J. Juan-Alcañiz, E.V. Ramos-Fernandez, K.B. Sai Sankar Gupta, E. Stavitski, H. van Bekkum, J. Gascon, F. Kapteijn, J. Catal. 281 (2011) 177–187.
[14] A. Dhakshinamoorthy, M. Alvaro, H. Garcia, J. Catal. 267 (2009) 1–4.
[15] V. Isaeva, L. Kustov, Pet. Chem. 50 (2010) 167–180.
[16] R.J. Kuppler, D.J. Timmons, Q.-R. Fang, J.-R. Li, T.A. Makal, M.D. Young, D. Yuan, D. Zhao, W. Zhuang, H.-C. Zhou, Coord. Chem. Rev. 253 (2009) 3042–3066.
[17] S. Opelt, S. Türk, E. Dietzsch, A. Henschel, S. Kaskel, E. Klemm, Catal. Commun. 9 (2008) 1286–1290.
[18] P. Serra-Crespo, E.V. Ramos-Fernandez, J. Gascon, F. Kapteijn, Chem. Mater. 23 (2011) 2565–2572.
[19] J. Juan-Alcañiz, E.V. Ramos-Fernandez, U. Lafont, J. Gascon, F. Kapteijn, J. Catal. 269 (2010) 229–241.
[20] Y.K. Hwang, D.-Y. Hong, J.-S. Chang, H. Seo, M. Yoon, J. Kim, S.H. Jhung, C. Serre, G. Férey, Appl. Catal., A 358 (2009) 249–253.
[21] Z. Saedi, S. Tangestaninejad, M. Moghadam, V. Mirkhani, I. Mohammadpoor-Baltork, Catal. Commun. 17 (2012) 18–22.
[22] E.V. Ramos-Fernandez, M. Garcia-Domingos, J. Juan-Alcañiz, J. Gascon, F. Kapteijn, Appl. Catal., A 391 (2011) 261–267.
[23] N.V. Maksimchuk, K.A. Kovalenko, S.S. Arzumanov, Y.A. Chesalov, M.S. Melgunov, A.G. Stepanov, V.P. Fedin, O.A. Kholdeeva, Inorg. Chem. 49 (2010) 2920–2930.
[24] N.V. Maksimchuk, M.N. Timofeeva, M.S. Melgunov, A.N. Shmakov, Y.A. Chesalov, D.N. Dybtsev, V.P. Fedin, O.A. Kholdeeva, J. Catal. 257 (2008) 315–323.
[25] N.V. Maksimchuk, O.A. Kholdeeva, K.A. Kovalenko, V.P. Fedin, Isr. J. Chem. 51 (2011) 281–289.
[26] N.V. Maksimchuk, O.V. Zalomaeva, I.Y. Skobelev, K.A. Kovalenko, V.P. Fedin, O.A. Kholdeeva, Proc. R. Soc. A. Roy. Soc. A Math. Phy. 468 (2012) 2017–2034.
[27] Y. Pan, B. Yuan, Y. Li, D. He, Chem. Commun. 46 (2010) 2280–2282.
[28] F.G. Cirujano, F.X. Llabrés i Xamena, A. Corma, Dalton Trans. 41 (2012) 4249–4254.
[29] F.G. Cirujano, A. Leyva-Pérez, A. Corma, F.X. Llabrés i Xamena, ChemCatChem 5 (2013) 538–549.
[30] J. Hermannsdörfer, R. Kempe, Chem. Eur. J. 17 (2011) 8071–8077.
[31] E.V. Ramos-Fernandez, C. Pieters, B. van der Linden, J. Juan-Alcañiz, P. Serra-Crespo, M.W.G.M. Verhoeven, H. Niemantsverdriet, J. Gascon, F. Kapteijn, J. Catal. 289 (2012) 42–52.
[32] M. Marchetti, S. Paganelli, E. Viel, J. Mol. Catal. A: Chem. 222 (2004) 143–151.
[33] M. Bortenschlager, J. Schütz, D. von Preysing, O. Nuyken, W.A. Herrmann, R. Weberskirch, Organomet. Chem. 690 (2005) 6233–6237.
[34] C.D. Frohning, C.W. Kohlpaintner, H.-W. Bohnen, in: B. Cornils, W.A. Herrmann (Eds.), Applied Homogeneous Catalysis with Organometallic Compounds—A Comprehensive Handbook in Three Volumes, second ed., Wiley-VCH, 2002, p. 31.
[35] M.S. Shaharun, B.K. Dutta, H. Mukhtar, S. Maitra, Chem. Eng. Sci. 65 (2010) 273–281.
[36] H.-W. Bohnen, B. Cornils, Advances in Catalysis, 47, Academic Press, Waltham, MA, 2002, pp. 1.
[37] P.C.J. Kamer, J.N.H. Reek, P.W.N.M. van Leeuwen, in: B. Heaton (Ed.), Mechanisms in Homogeneous Catalysis, A Spectroscopic Approach, Wiley-VCH, Weinheim, 2005, p. 231.
[38] S.K. Sharma, P.A. Parikh, R.V. Jasra, J. Mol. Catal. A: Chem. 316 (2010) 153–162.
[39] S. Alini, A. Bottino, G. Capannelli, A. Comite, S. Paganelli, Appl. Catal., A 292 (2005) 105–112.
[40] D. Cauzzi, M. Lanfranchi, G. Marzolini, G. Predieri, A. Tiripicchio, M. Costa, R. Zanoni, J. Organomet. Chem. 488 (1995) 115–125.
[41] H. Gao, R.J. Angelici, J. Mol. Catal. A: Chem. 145 (1999) 83–94.
[42] J. Balué, J.C. Bayón, J. Mol. Catal. A: Chem. 137 (1999) 193–203.
[43] D.E. Bryant, M. Kilner, J. Mol. Catal. A: Chem. 193 (2003) 83–88.
[44] S.-I. Fujita, S. Akihara, S. Fujisawa, M. Arai, J. Mol. Catal. A: Chem. 268 (2007) 244–250.
[45] T.A. Zeelie, A. Root, A.O.I. Krause, Appl. Catal., A 285 (2005) 96–109.
[46] J. Yang, Q. Zhao, J. Li, J. Dong, Microporous Mesoporous Mater. 130 (2010) 174–179.

[47] G. Porod, in: O. Glatter, O. Kratky (Eds.), Small Angle X-Ray Scattering, Academic Press, London, 1982.
[48] A.C. Geiculescu, H.J. Rack, J. Non-Cryst. Solids 306 (2002) 30–41.
[49] J. Schäffer, V.A. Kondratenko, N. Steinfeldt, M. Sebek, E.V. Kondratenko, J. Catal. 301 (2013) 210–216.
[50] D.-Y. Hong, Y.K. Hwang, C. Serre, G. Férey, J.-S. Chang, Adv. Funct. Mater. 19 (2009) 1537–1552.
[51] I. Ogino, B.C. Gates, Phys. Chem. C 114 (2010) 2685–2693.
[52] I. Ogino, C.-Y. Chen, B.C. Gates, Dalton Trans. 39 (2010) 8423–8431.
[53] W.J. Mortier, Compilation of Extra-Framework Cation Sites in Zeolites, Butterworth Scientific Ltd. (on behalf of the Structure Commission of the International Zeolite Association), Surrey, UK, 1982.
[54] T.V. Vu, H. Kosslick, A. Schulz, J. Harloff, E. Paetzold, J. Radnik, U. Kragl, G. Fulda, C. Janiak, N.D. Tuyen, Microporous Mesoporous Mater. (2013), http://dx.doi.org/10.1016/j.micromeso.2013.02.035.
[55] J. Patel, S. Mujcinovic, W.R. Jackson, A.J. Robinson, A.K. Serelis, C. Such, Green Chem. 8 (2006) 450–454.